Renewable Energy 256 (2026) 124305

Contents lists available at ScienceDirect

Renewable Energy

journal homepage: www.elsevier.com/locate/renene

Quasi-passive reactance control for two-body axisymmetric heaving WECs☆

Marco Alves [a], António Sarmento [a], Marcos Blanco [b,*], Miguel Vicente [a], Mário Vieira [a], Marcos Lafoz [b]

[a] *WavEC- Offshore Renewables, Portugal*
[b] *Ciemat-Centro Investigaciones Energéticas, Medioambientales Y Tecnológicas, Spain*

ARTICLE INFO

Keywords:
Wave energy
WEC
Point absorber
Quasi-passive reactance control
WEC resonance
Mass-transfer mechanism

ABSTRACT

Ocean wave energy has the potential to play a key role in a low-carbon future due to its vast untapped resources. However, Wave Energy Converters (WECs) remain at a pre-commercial stage and must improve competitiveness by enhancing reliability, lowering LCOE, and increasing energy generation. The latter can be achieved by shifting from damping controls to reactance controls, optimizing WEC-wave mechanical resonance to boost energy output. In this context, a novel quasi-passive reactance control concept is introduced, incorporating a physical mass transfer system rather than relying solely on control algorithms to supply reactive energy to the WEC. The paper presents the concept, a phenomenological discussion and the supporting mathematical theory applied to a spar-type axisymmetric two-body heaving point absorber that incorporates a mass transfer mechanism to control the reactance. Point absorbers, by their nature, usually have very narrow frequency responses and quite often their peak frequency response is much higher than the typical wave frequencies. The proposed quasi-passive reactance control significantly broadens the frequency response bandwidth to align it with typical ocean wave frequencies, enhancing energy extraction to optimal reactance levels and thereby increasing annual energy yield. The key finding of this analysis is that, when well controlled, the proposed mass transfer mechanism can increase the power capture bandwidth by more than three times compared to the baseline case without the mechanism.

1. Introduction

The transition to a low carbon future in which clean, affordable, renewable electricity powers the world is an ongoing process that will require the complementary contribution of different renewable sources to the energy mix. Whilst hydro, solar and wind power (onshore and offshore) are currently the main renewable energy sources worldwide [1], wave power is still an untapped resource and harnessing wave energy still presents, among others, several technical and economic challenges. In the last few decades, engineers and scientists have been tackling these challenges to find the most cost-effective way to harness ocean energy. However, harsh sea conditions have hampered the development of resilient and reliable technologies able to solve the challenges of generating affordable power from the oceans. Despite that, the high potential of this inexhaustible energy source (the worldwide potential of wave energy is estimated at around 2 TW [2]) unveils a great potential for conversion into useful power and to become a prominent share of the renewable energy mix across the world. In Europe, the Commission assessed offshore renewable energy (ORE) decarbonization scenarios for the European Green Deal's 2050 climate neutrality target [3], highlighting wave energy as a promising source with a projected 31 GW capacity by 2050 [4], contingent on strong industry support.

Beyond utility-scale power production, wave energy can offer a cost-effective solution for microgrids, supporting remote islands and coastal communities (e.g., Canary and Caribbean Islands) by replacing costly, polluting diesel-based generation and enhancing energy independence through local resources. Furthermore, Wave energy can power offshore industries like aquaculture, oil & gas, hydrogen electrolysis, and reverse osmosis desalination, addressing global clean water needs [5]. According to the World Resources Institute, 25 countries, which collectively account for one-quarter of the global population, are currently experiencing extremely high water stress on an annual basis [6].

However, despite its promise, wave energy faces several cost-effectiveness challenges compared to other renewables, from

☆ During the preparation of this work the author(s) used CHATGPT in order to improve readability and language in the writing process. After using this tool/service, the author(s) reviewed and edited the content as needed and take(s) full responsibility for the content of the publication.

* Corresponding author. Avda. Complutense 40, CP 28040, Madrid, Spain.
E-mail address: marcos.blanco@ciemat.es (M. Blanco).

https://doi.org/10.1016/j.renene.2025.124305
Received 20 May 2025; Received in revised form 22 August 2025; Accepted 22 August 2025
Available online 23 August 2025
0960-1481/

technology design to operation and maintenance. In this respect, Ocean Energy Systems (OES) proposes eight evaluation areas in which ocean renewables must be evaluated for its market readiness: affordability, power capture and conversion, controllability, reliability, survivability, maintainability, installability and manufacturability [7]. Power capture, conversion and controllability are deemed as the most daunting, as the variability of this renewable source challenges the rigorous restrictions of electric grid stability. Primarily due to the reciprocating motion induced by ocean waves and the variability of the resource, power produced by wave energy converters (WECs) is normally more uneven than other renewable sources. Resource variability causes large peak-to-average power fluctuations [8] (a feature especially associated with wave energy converters employing linear generators [9]), increasing grid integration costs and requiring oversized WEC generators and power electronics when a reactive control is implemented [10] (making them more expensive to build), and must also be considered in the sizing of transmission cables due to the associated current ratings and thermal constraints [11]. Nevertheless, these fluctuations are expected to be mitigated in a farm with tens or hundreds of converters exporting power to shore [12], as the power output will be much smoother due to phase and amplitude cancellation when a proper farm planning is implemented [13]. This issue affects WEC performance to varying extents, depending on the operating principle; it could be particularly pronounced in direct-drive power-take-off (PTO) [14], while it can be tackled more easily in oscillating water columns (OWC) as the air turbine's flywheel effect stores kinetic energy, enabling smoother mechanical-to-electrical conversion and filtering power oscillations [15].

Given the variability of wave resources and the strict grid constraints, WEC control is crucial for maximizing and stabilizing power output while adhering to grid code requirements [16]. Apart from the grid restrictions, each of the components of WECs might add extra constraints to the conversion process, such as force, displacement, or speed limitations. In general, these components are designed to perform more efficiently close to nominal conditions, losing performance when operating far from these design conditions. Furthermore, component's design must guarantee reliability by ensuring that fatigue failure does not happen before the lifespan, while ensuring survivability in harsh offshore conditions as well. Therefore, design approaches must balance these constraints with cost-benefit trade-offs to enhance market competitiveness.

Eventually, the path to wave energy commercialization hinges on lowering the levelized cost of energy (LCOE) by reducing OpEx, CapEx, and capital costs while enhancing power generation. Cost reduction involves new materials, cheaper components, efficient manufacturing, optimized logistics, and improved WEC reliability. Increasing power output requires better WEC response across spectral frequencies. This involves broadening the absorption bandwidth, which can be achieved by controlling more effectively the system's reactance to improve its resonance characteristics. Different design strategies, based on the same principle, have been adapted to concepts varying in scale, visibility, power-take-off system, and working principle, ranging from capturing the wave's up-and-down (heave) movement to its to-and-fro (surge) motion to drive the power-take-off system.

This study focuses on point absorber WECs, as they represent the most promising technologies under development. Point absorbers are characterized by a length much smaller than the wavelength, resulting in hydrostatic restoring forces dominating over inertia. Using the electric analogue [17], their mechanical reactance is primarily capacitive (i.e. the ability of the hydrostatic spring to store potential energy), while inductive reactance (i.e. the inductance or mass's ability to store kinetic energy) is less relevant in the most energetic sea frequencies. This poses a challenge for the WEC design, as canceling system reactance requires a spring force acting with, rather than against, motion - complicating resonance-based tuning and control.

Point absorbers fall into two main types: single-body systems reacting against a fixed seabed point and two-body systems utilizing relative motion between the two bodies for energy conversion. This study focuses on the latter, though findings also apply to single-body systems. Building on previous research [18], which demonstrated that, assuming linearity, a two-body system is equivalent to a one-mode, one-body system, this study applies the electric analogue approach [19], and Thevenin's theorem [20] to evaluate power absorption in spar-type axisymmetric two-body heaving systems. It examines conditions under which these systems can achieve the theoretical maximum power absorption of a single body heaving point absorber while using a power take-off mechanism that restricts only relative motion.

This work also presents and analyzes a conceptual mass transfer mechanism (MTM) that shifts mass between the two bodies based on relative displacement, helping control WEC reactance to improve energy capture and expand the typically narrow bandwidth of point absorbers. Studies on reactance control [21] are usually focused on frequency domain formulations of impedance-based control [22], or time domain implementations of advanced control techniques, such as model predicted control [23], deep reinforcement learning [24], or inverse fuzzy model control [25], but without any additional mechanism to actively change the hydrodynamics of the WECs. Mechanical approaches based on the inclusion of additional systems focused on forcing the mechanical resonance (to enhance power capture and/or bandwidth) has been analyzed, such as biostable mechanic systems [26], double linear generators coupled by springs [27], a compressible degree of freedom using air volumes [28], or a 2:1 heave-to-pitch WEC coupled with a pendulum [29]. The proposed MTM are framed in the latter, with a novel proposal of inclusion of an additional systems, and the analysis carried out presents the energy extraction analysis in frequency domain. Optimal (reactance) control - control that maximizes the mechanical energy extracted from the waves - is typically formulated in the frequency domain and expressed as an optimal impedance value [17]. Alternative frequency formulations of this optimal control strategy have been proposed, where the control law is expressed in terms of a force command -instead of an impedance value- and in terms of electric power in order to account for PTO losses [30] and to address maximum force, velocity limitations or avoid end-stop collisions [31]. Expansions of the frequency-domain equations to account for additional effects, such as mooring dynamics, as well as the coupling of heave motion with other degrees of freedom has been considered too [19]. The present study extends the frequency-domain formulation by incorporating the additional terms associated with the additional systems that introduce the MTM technique (the change in the equations' parameters due to mass transfer), changing the optimal control equations in consequence. This technique for controlling reactance is expected to boost power generation and quality by enabling energy absorption across a wider range of wave frequencies, reducing peak-to-average power variations and smoothing output. However, as noted at the end of this paper, further research is needed to evaluate the effectiveness and practicability of the proposed design approach.

2. Phenomenological discussion

Most of point absorber concepts under development are axisymmetric floating devices and its working principle is based on the vertical motion of a body or the relative motion between two bodies oscillating in the same mode, heave in most cases [6,32]. For this reason, it is the type of device that we consider in this analysis, namely spar-type axisymmetric two-body self-reacting heaving systems (see Fig. 1). This implies that: the floater (body 1) is force reacting against a reaction spar (body 2), formed by a vertical structure rigidly connected to a submerged mass (or an inertial plate with an equivalent effect). The PTO equipment can include mechanical systems like a rack and pinion or a hydraulic system driving a rotating generator, or direct-drive linear generators, among others [14,33]. The study consists of an analytical assessment supported by numerical simulations using the numerical tool

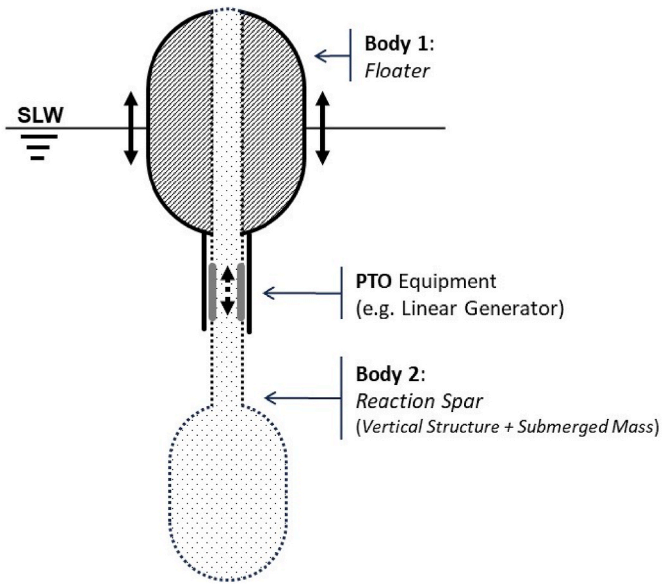

Fig. 1. Schematic representation of the two-body spar-type WEC considered in this study: a self-reacting heaving system consisting of a surface body or floater (body 1) that reacts against a spar former by a vertical structure connected to a submerged mass (body 2).

WAMIT, a 3D boundary element code based on linear wave theory, widely used to analyze wave-structure interactions in offshore environments [34]. WAMIT employs the boundary element method (BEM) to solve wave loads and motions through a potential flow model with linear boundary conditions. WAMIT is widely used in the industry and has been extensively validated through experimental data.

When analyzing a WEC merely in its energy-extracting mode (1-DOF) (heave in this study), mooring loads are typically neglected, as the mooring system primarily ensures positional stability without significantly impacting energy capture. This simplification allows clearer assessment of how test parameters affect WEC performance. Although the methodology used here focuses on the concepts mentioned above, it can easily be extended to cover other types of wave energy converters and operating principles based on other energy-extracting modes.

2.1. Two-body systems

This study presents a conceptual theoretical analysis of mass transfer as a strategy to broaden the capture bandwidth of a spar-type, axisymmetric two-body heaving point absorber. Practical implementation is not addressed here but will be explored in future work, focusing on two classes of spar-type WECs: force-reacting systems and floating oscillating water columns (OWCs). For floating OWCs, mass transfer can be readily engineered by redesigning the structure to include an aperture in the spar tube within the top floater, enabling bidirectional water flow between the water column (body-2) and the surrounding structure (body-1). In contrast, implementation in self-reacting two-body point absorbers is likely more complex. One possible approach involves channeled water tanks that transfer water between reservoirs based on their relative positions. Alternatively, transferring fluids denser than water could amplify the desired effect with smaller volumes, offering a more compact solution.

In the following analysis, the heave velocities of the two bodies are denoted by $u_3(t)$ for body 1 and $u_9(t)$ for body 2, and the heave excitation forces, caused by incident waves assuming that both bodies are still, are represented by $f_3(t)$ and $f_9(t)$. Their Fourier-transformed counterparts (functions of the angular frequency ω) are denoted by U_3, U_9, F_3 and F_9, respectively. In accordance, the mass and hydrostatic buoyancy are given by m_3 and C_3 for body 1 and m_9 and C_9 for body 2. The notation used herein is consistent with WAMIT [34] and NEMOH [35], where the indices 3 and 9 correspond to the heave mode of body 1 and body 2, respectively.

For the sake of clarity of the mathematical formulation, it is convenient to define the velocity and excitation force vectors as two-dimensional column vectors, that is,

$$\mathbf{U} = \begin{bmatrix} U_3 \\ U_9 \end{bmatrix} \text{ and } \mathbf{F_e} = \begin{bmatrix} F_3 \\ F_9 \end{bmatrix}. \tag{1}$$

In addition to the excitation force F_e caused by the incoming waves in both bodies 1 and 2, there is an added force on the captor generated by the oscillatory motions. Whenever the bodies oscillate, a wave is radiated. This force, called radiation force, F_r, is given by,

$$\mathbf{F_r} = -\mathbf{Z}\mathbf{U}, \tag{2}$$

where $\mathbf{Z}$ represents the radiation impedance matrix, a transfer function of a linear system where $\mathbf{U}$ and $\mathbf{F_r}$ are the system input and output, respectively. The radiation impedance can be written as

$$\mathbf{Z} = \begin{bmatrix} Z_3 & Z_{39} \\ Z_{93} & Z_9 \end{bmatrix} = -\mathbf{B} + i\omega\mathbf{A}, \tag{3}$$

where, $\mathbf{B}$ is the radiation resistance matrix (real part of $\mathbf{Z}$), and $\mathbf{A}$ the hydrodynamic added mass matrix ($\omega\mathbf{A}$ is the imaginary part of $\mathbf{Z}$). Therefore, the radiation force embodies a resistive term, proportional to the velocity complex amplitude, and an inertial term, proportional to the acceleration complex amplitude. The damping coefficient is thus related to the time average energy flux transmitted to the fluid by the body oscillations, which propagates away from the body. The energy involved in this process is resistive as it is associated with a damping effect. On the other hand, the added mass coefficient corresponds to an inertial increment due to the water displaced in the body vicinity when the body moves. The energy involved in this process is reactive as it flows alternately between the body and the fluid. According to the electrical analogy explored later, the added mass and the damping coefficients represent radiation reactance and radiation resistance effects, respectively.

It should be noted that $\mathbf{Z}$, $\mathbf{B}$ and $\mathbf{A}$ are symmetric matrices. The matrix elements Z_{39} and Z_{93} (commonly referred as Z_c) represent the hydrodynamic radiation coupling between the two bodies.

In the connection between the two bodies the PTO mechanism is incorporated to convert mechanical energy into electricity and to control the performance of the WEC to achieve maximum energy conversion under different sea states. The PTO equipment (not specified here), supplies a force, $\mathbf{F_{pto}}$, given by

$$\mathbf{F_{pto}} = -Z_{pto}(U_3 - U_9) = -Z_{pto}U_r, \tag{4}$$

where Z_{pto} is a complex load impedance and U_r the relative velocity. The sign of $\mathbf{F_{pto}}$ is chosen so that it adds and subtracts to the heave force on bodies 1 and 2, respectively. If the PTO is passive, supplying a purely resistive load (i.e., with no reactance), Z_{pto} is purely real, representing only a mechanical load resistance.

For a more realistic system representation, viscous loss can be incorporated into the dynamics. In a linear system, it is modeled as proportional to velocity, with loss resistance as the proportionality constant (i.e., $\mathbf{F_{v_j}} = -V_i U_j$, with $j = 3, 9$ being V_i is the loss resistance). However, for simplicity, we neglect, as before, the viscous forces in the discussion that follows.

Eventually, the linear-system model of a two-body WEC is expressed, in matrix form, by the motion equations,

$$\begin{bmatrix} Z_3 + Z_{pto} & Z_c - Z_{pto} \\ Z_c - Z_{pto} & Z_9 + Z_{pto} \end{bmatrix} \begin{bmatrix} U_3 \\ U_9 \end{bmatrix} = \begin{bmatrix} F_3 \\ F_9 \end{bmatrix}, \tag{5}$$

where, besides the PTO load impedance, Z_{pto}, we have introduced the diagonal elements of the impedance matrix, Z_k for $k = \{3, 9\}$, and the cross-coupling (off-diagonal) elements $Z_c = Z_{39} = Z_{93}$. These impedances are decomposed into their real (resistive) parts, R, and imaginary (reactive) parts, X, as,

$$Z_k = R_k + iX_k, \text{for } k = \{3, 9\}, \text{and } Z_c = R_c + iX_c, \tag{6}$$

where the resistive components are given by,

$$R_k = B_{kk}, \text{and } R_c = B_{39} = B_{93}, \tag{7}$$

and the reactive components obtained from,

$$X_k = \omega\left(m_k + A_{kk} - \frac{C_k}{\omega^2}\right), \text{and } X_c = \omega A_{39} = \omega A_{93}. \tag{8}$$

The impedances Z_3 Z_9 and Z_c are independent of the load impedance Z_{pto}, and so they represent intrinsic (hydrodynamic and hydrostatic) properties of the two-body system.

2.2. Equivalent single-body system

This subsection develops the one-body equivalent model for the two-body WEC using Thévenin's theorem [20,30], a fundamental principle in electrical circuit analysis. The approach aligns with J. Falnes' work on wave energy conversion through the relative motion of two single-mode oscillating bodies [18]. This equivalent model offers two main advantages: (1) it allows direct comparison of energy extraction performance between single-body systems (e.g., point absorbers reacting against the seabed) and two- or multi-body systems (e.g., two-body point absorbers or floating OWC devices); and (2) it enables the application of energy extraction and optimal control formulations, originally developed for single-body systems, to two-body configurations. To achieve this, the total excitation force on both bodies is determined (i.e. the wave force when both bodies are fixed) by summing the two scalar equations in the matrix, Eq. (5), yielding,

$$(Z_3 + Z_c)U_3 + (Z_9 + Z_c)U_9 = F_3 + F_9. \tag{9}$$

Note that the summation of the two scalar equations eliminates the mechanical load impedance, Z_{pto}, from the left-hand side of Eq. (9). When $Z_{pto} \rightarrow \infty$ the two bodies are bound to move together as a single combined body and so $U_9 = U_3 = U_0$. In this case, Eq. (9) assumes the form

$$Z_0 U_0 = F_3 + F_9 = F, \tag{10}$$

where

$$Z_0 = Z_3 + Z_9 + 2Z_c \tag{11}$$

represents the mechanical impedance of the combined body. If the impedance $Z_0 \neq 0$, Eq. (10) shows that $U_0 = 0$ in the case of ideal force compensation, i.e. $F_9 = -F_3$. To allow large relative motions without causing significant nonlinearities (e.g., due to significant variations in the floater's water-plane area or large displacements), the WEC design should enable U_0 to be relatively small, which means either small F (approximate force compensation) or large Z_0.

The PTO force exerted between the two bodies may be rewritten as

$$F_{pto} = -\frac{1}{2}(F_3 - F_9 - Z_3U_3 + Z_9U_9 + Z_cU_r), \tag{12}$$

which is obtained by subtracting the two scalar equations represented in matrix Eq. (4). Using Eq. (12), the force induced by the waves on the connecting interface when both bodies are rigidly connected (i.e., when $Z_{pto} \rightarrow \infty$), is obtained from

$$F_0 = -F_{pto\,(Z_{pto}\rightarrow\infty)} = \frac{1}{2}[F_3 - F_9 - (Z_3 - Z_9)U_0] = \frac{F_3(Z_9 + Z_c) - F_9(Z_3 + Z_c)}{Z_0}. \tag{13}$$

Furthermore, by solving the 2×2 system of scalar equations, Eq. (5), and combining the result with Eq. (13), the relative velocity, $U_r = U_3 - U_9$, can be expressed as

$$U_r = \frac{F_3(Z_9 + Z_c) - F_9(Z_3 + Z_c)}{Z_3Z_9 - Z_c^2 + Z_0Z_{pto}} = \frac{F_0}{Z_i + Z_{pto}}, \tag{14}$$

where Z_i is given by

$$Z_i = \frac{Z_3Z_9 - Z_c^2}{Z_0} = \frac{Z_3Z_9 - Z_c^2}{Z_3 + Z_9 + 2Z_c}. \tag{15}$$

Eq. (14) yields the very useful one-body equivalent model for the two-body WEC, where F_0 represents the equivalent excitation force, i.e., the wave-induced force in the connection between the two bodies when there is no relative motion ($U_3 = U_9 = U_0$), which occurs when $Z_{pto} \rightarrow \infty$. Furthermore, Z_i denotes the equivalent intrinsic impedance, i.e., the ratio between F_0 and U_r when $Z_{pto} = 0$. In this case, the force applied between the two bodies vanishes, $Z_{pto} = 0$, and so there is no mechanical, but only hydrodynamic coupling between the two bodies.

2.3. Simplification of the one-body WEC equivalent model

For two-body WECs, as with one-body systems, the energy harvested is maximized when the wave-induced force on the connection between the two bodies, F_0, and the relative velocity, U_r, are in phase. To explore this possibility, it is convenient to first evaluate the system's dynamics without a PTO in the connection between the two bodies. In this case, by applying Eq. (6), Eq. (14) expands as follows

$$U_r = \frac{F_0}{Z_i} = \frac{[F_3(R_9 + R_c) - F_9(R_3 + R_c)] + i[F_3X_9 - F_9X_3 + X_c(F_3 - F_9)]}{[R_3R_9 - R_c^2 - X_3X_9 + X_c^2] + i[R_9X_3 + R_3X_9 - 2R_cX_c]}. \tag{16}$$

Examining Eq. (16) provides insights into the factors that influence energy maximization. To this end, we first examined the **real part of the numerator** of Eq. (16), which can easily be concluded to be zero. By combining the Haskind relation, which establishes an alternative way to compute the excitation force using the radiation potential (either at the body wet surface or at a control surface in the far-field region [17]), with the reciprocity relation, which defines the radiation-resistance matrix[1] in terms of far-field quantities (based on the principle that the energy radiated from an oscillating body can be losslessly recovered in the far-field region, assuming an ideal fluid), the radiation-resistance matrix for an axisymmetric two-body WEC constrained to vertical oscillations can be expressed as

$$B_{ij} = \frac{k}{8J}F_iF_j^*, \tag{17}$$

where the indices i and j refer to the vertical degrees-of-freedom (DOF) of the floater (body 1) and the reaction spar (body 2), denoted commonly by the subscript 3 and 9, respectively. In this case, the diagonal terms of the radiation matrix reduce to $B_{33} = k/8J|F_3|^2$ and $B_{99} = k/8J|F_9|^2$.

Considering the simplified form of the radiation-resistance matrix, Eq. (17), it can be concluded, after straightforward mathematical manipulations, where viscous effects are neglected (i.e., $R_3 = B_{33}$), that the real part of the numerator of the relative velocity, Eq. (16), cancels out, i.e.,

[1] The radiation-resistance matrix in Eq. (17) is a special case of a general expression that establishes a direct relationship between a body's ability to radiate waves in a given direction and the excitation force exerted by an incident plane wave from the same direction. It is given by.

$$B_{ij} = \frac{k}{16\pi J}\int_{-\pi}^{\pi} F_i(\beta)F_j^*(\beta)$$

$$F_3(R_9 + R_c) - F_9(R_3 + R_c) = 0. \tag{18}$$

Further simplifications arise because, for small bodies (point absorbers), radiation impedance is typically dominated by radiation reactance, i.e., $X_{ij} \gg R_{ij}$. Additionally, off-diagonal (cross-coupling) hydrodynamic coefficients are usually much smaller than the diagonal (direct) terms, i.e., $B_{33} \gg B_{39} \ll B_{99}$ and $A_{33} \gg A_{39} \ll A_{99}$. This last aspect is particularly emphasized in the design approach explored in this study, in which the two bodies of the point absorber tend to be quite apart (see Fig. 1). With these simplifications, the **real part of the denominator** of the relative velocity in Eq. (16) reduces to

$$R_3R_9 - R_c^2 - X_3X_9 + X_c^2 \cong -X_3X_9. \tag{19}$$

Furthermore, considering once again that the cross-coupling hydrodynamic coefficients are negligible when compared to the diagonal elements, the **imaginary part of the numerator** of the relative velocity, Eq. (16), takes the simplified form,

$$F_3X_9 - F_9X_3 + X_c(F_3 - F_9) \cong F_3X_9 - F_9X_3. \tag{20}$$

The point absorber design approach discussed here is based on the principle that the floater serves as the primary structural component responsible for the wave-radiation pattern, i.e. $R_3 \gg R_9 \gg R_c$, and thus, according to the Haskind's relation, $F_3 \gg F_9$ (see Eq. (17)), we might conclude that $F_3X_9 \gg F_9X_3$, suggesting that a further simplification could be made by neglecting the term F_9X_3. This is true to some extent, except at low frequencies where the excitation force (per unit incident wave amplitude) on heaving bodies approaches the hydrostatic restoring coefficient, which physically means that the whole device moves with the wave for long waves. In addition, when the frequency approaches zero, the intrinsic reactance can be considerably high since it is dominated by the capacitive reactance, C_3/ω, which would increase up to infinity (for low frequencies the inductive reactance, $\omega(m_9 + A_{99})$, is cancelled). Therefore, neglecting the term F_9X_3 is often an overly simplistic approximation and so the two imaginary components, $F_3X_9 - F_9X_3$, must be considered.

Finally, evaluating the **imaginary part of the denominator** reveals that the term R_3X_9 is dominant over the other two terms, which allows the simplification,

$$R_9X_3 + R_3X_9 - 2R_cX_c \cong R_3X_9. \tag{21}$$

This simplification results from the fact that the wave-radiation pattern is mainly driven by the floater's dynamics, given that $R_3 \gg R_9$, and the off-diagonal hydrodynamic coefficients are significantly smaller than the diagonal elements, as noted above. Therefore, the cross-coupling reactance, X_c, which consists only of an inductive reactance term, ωA_{39}, is less relevant that the intrinsic inductive reactance of the floater, $\omega(m_3 + A_{33})$, or the reaction spar, $\omega(m_9 + A_{99})$. Thus, since $R_3 \gg R_c \ll R_9$, the term $2R_cX_c$ can be disregarded whenever the design approach followed here is applied. Furthermore, since R_9 has minimal impact on the two-body equivalent resistance, R_9X_3 can also be disregarded. This is expected, as the resistance, R_9, decreases to zero at low frequencies, which offsets the increase of the reactance, X_3, caused by the augment of the capacitive reactance, C_3/ω, up to infinity as the frequency approaches zero. The radiation cancels for long waves because the device oscillates in sync with the free surface elevation, resulting in no relative motion between the waves and the device. This means that the excitation force is in phase with the displacement, resulting in a null resistive component of the impedance.

To justify their application, Fig. 2 confirms the validity of the assumptions and simplifications previously discussed for axisymmetric two-body self-reacting WECs oscillating vertically. The top-left quadrant decomposes the real part of the numerator of Eq. (16), confirming that it is inherently zero. The remaining quadrants compare the imaginary and real parts of the denominator, as well as the imaginary parts of the numerator, with the simplified expressions derived from the preceding discussion (indicated by white dots), showing that the differences are negligible.

Eventually, introducing the simplifications discussed above in the relative velocity, U_r, expressed by Eq. (16), the one-body equivalent model for the two-body WEC degenerates into

$$U_r = \frac{i[F_3X_9 - F_9X_3]}{-X_3X_9 + iR_3X_9}. \tag{22}$$

The term R_9X_3 is disregarded in the imaginary part of the

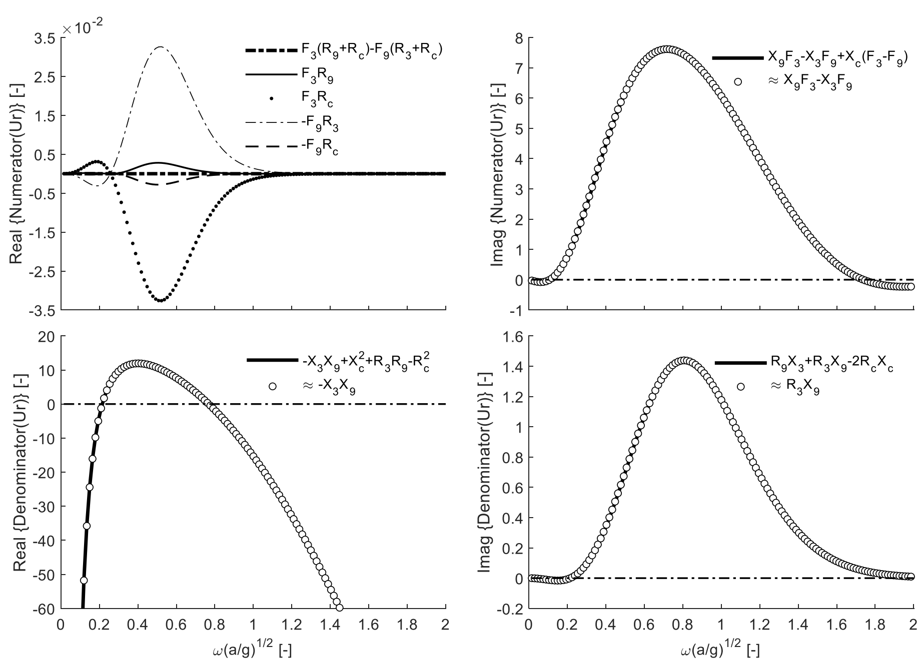

Fig. 2. Axisymmetric two-body self-reacting heaving WECs. Graphic representation of the magnitude of the real and imaginary parts of the denominator and numerator of the complex amplitude of the relative velocity, considering the simplifications stressed above: Breakdown of the real part of the numerator into its components (top left); original and simplified form of the imaginary part of the numerator (top right); original and simplified form of the real part of the denominator (bottom left); original and simplified form of the imaginary part of the denominator (bottom right).

denominator, while F_9X_3 is retained in the numerator of Eq. (22), because the hydrodynamic damping at low frequencies tends to zero (for long waves the body follows the movement of the free surface and thus it is unable to radiate waves), while the excitation force tends to the hydrostatic coefficient (for unit amplitude waves). However, except at low frequencies, the term F_9X_3 is of minor importance, primarily due to the relatively low dynamic pressure at the deep location of the reaction spar.

3. Quasi-passive reactance control by means of an MTM

Point absorber WECs are defined by a characteristic length, typically the diameter, much smaller than the incoming wavelength, as noted before. This makes hydrostatic restoring forces dominant over inertia forces at common wave frequencies, leading the mechanical reactance to be predominantly capacitive, with little inductive reactance influence. Making use of the electric analogue [17,18], the capacitive reactance can be seen as the ability of the hydrostatic spring to store potential energy and conversely the inductive reactance as the mass's ability to store kinetic energy.

$$U_r = \frac{[F_3(R_9+R_c) - F_9(R_3+R_c)] + i[F_3X_9 - F_9X_3 + X_c(F_3-F_9)]}{\left[\left(R_3R_9 - R_c^2 - X_3X_9 + X_c^2\right) - \frac{\Gamma}{\omega}(X_3+X_9+2X_c)\right] + i\left[\left(R_9X_3 + R_3X_9 - 2R_cX_c\right) + \frac{\Gamma}{\omega}(R_3+R_9+2R_c)\right]}, \tag{26}$$

In the discussion that follows we consider a mass transfer mechanism (MMT) as an alternative technique to control de reactance of two-body axisymmetric self-reacting WECs oscillating vertically, that consists of moving mass back and forth from one body to the other, depending on the relative displacement between them. Conceptually, different materials with different densities can be considered to maximize the intended effect. The variable mass of the body/ies due to the transfer mechanism is given by

$$m(t) = m_0 - \widehat{m}_t e^{i\omega t} \tag{23}$$

where m_0 represents the mass of the body/ies in undisturbed conditions and $\widehat{m}_t$ the complex amplitude of the oscillating mass between both bodies. The mass transfer has an impact on the system capacitive reactance, since it changes the hydrostatic restoring effect, and on the inductive reactance, as the kinetic energy stored also changes with the variation of the body mass. The oscillating mass term in Eq. (23) generates a second-order inertial term (the new mass term times acceleration), which is neglected according to linear theory, as assumed in this work. Therefore, the effect of the transfer mass in the inductive reactance is negligible. Reevaluating the hydrostatic restoring force is needed to assess the oscillating mass's impact on capacitive reactance, as it alters the balance between weight, W, and buoyancy, I. The next subsection details this reassessment.

3.1. Hydrostatic restoring force

In self-reacting two-body systems, the amended hydrostatic restoring force due to the MTM is given (for sinusoidal waves) by

$$f_{hs_i}(t) = W - I = g\left(m_{0_i} - \widehat{m}_t e^{i\omega t}\right) - g\left(m_{0_i} - \rho S_i \widehat{z}_i e^{i\omega t}\right), \tag{24}$$

where W represents the body weight and I its buoyancy. Furthermore, S_i embodies the body water-plane area and $\widehat{z}_i$ the complex amplitude of the body vertical displacement, in which the index i denotes body one ($i = 3$, the floater), or body two ($i = 9$, the reaction spar). From, Eq. (24) it follows that the complex amplitude of the hydrostatic force, takes the form

$$\widehat{F}_{hs_i} = \rho g S_i \widehat{z}_i - \Gamma\left(\widehat{z}_i - \widehat{z}_j\right) = \rho g S_i \widehat{z}_i - \Gamma \widehat{z}_r, \tag{25}$$

in which the term $\Gamma\widehat{z}_r = g\widehat{m}_t$ represents the correction to the hydrostatic force due to the mass transfer between the two bodies. Here, Γ is the mass transfer coefficient and $\widehat{z}_r = \widehat{z}_3 - \widehat{z}_9$ denotes the complex amplitude of the relative displacement. To some extent, Γ acts as a reduction in the hydrostatic restoring coefficient, improving the WEC tuning for a more effective response to incoming waves with a better balance between energy content and occurrence probability. This effect could be amplified by using a smaller volume of high-density material, achieving the desired mass transfer more efficiently.

The modification of the hydrostatic restoring force caused by mass transfer changes the reactance characteristics of the bodies (including the cross-coupling reactance), thereby impacting the dynamic behavior of the WEC and its relative velocity. By combining Eq. (14) with the impedance equations, Eq. (6), the modified relative velocity, U_r, due to mass transfer can be expressed in its expanded form as,

where Γ/ω is the capacitive reactance associated to the MTM. By examining Eq. (26), as done with Eq. (16), we can observe that the real and imaginary parts of the numerator (relat2ed to the excitation force on the WEC) remain unchanged, since the cross-coupling effect caused by the mass transfer between the two bodies cancels mutually. On the other hand, both the real and imaginary parts of the denominator (related to the intrinsic floating body resistance and reactance, respectively) will be modified due to changes in the restoring force, and thus in the natural response of the two-body system. According to the simplifications/assumptions discussed in subsection 2.1.2, based on the lower relevance of the off-diagonal coefficients when compared to the diagonal terms in the point absorber design approach considered here, we can rewrite Eq. (26) in a simplified form as

$$U_r = \frac{i(F_3X_9 - F_9X_3)}{\left[-X_3X_9 - \frac{\Gamma}{\omega}(X_3+X_9)\right] + i\left[R_3X_9 + \frac{\Gamma}{\omega}(R_3+R_9)\right]}. \tag{27}$$

Theoretically, we can consider a system in which the equivalent excitation force is in phase with the relative velocity, effectively canceling the reactance through a well-suited characterization of the mass transfer coefficient between the two bodies. This occurs whenever,

$$-X_3X_9 - \frac{\Gamma}{\omega}(X_3+X_9) \cong 0. \tag{28}$$

It may appear that the equivalent excitation force is in phase with the relative velocity when the denominator of Eq. (27) becomes real. However, this is not the case, as both the numerator and denominator must be divided by the combined body's mechanical impedance, Z_0, to properly represent the equivalent excitation force and inherent impedance (see Eq. (15)). It turns out that Z_0 is approximately imaginary because, as previously noted, the radiation impedance for small bodies is largely dominated by the radiation reactance (i.e., $X_{ij} \gg R_{ij}$) and the off-diagonal hydrodynamic coefficients are generally much smaller than the diagonal terms. That said, the inherent impedance is real, and thus the excitation force is in phase with the relative velocity, whenever the real term, not the imaginary term, of the denominator in Eq. (27) is canceled.

According to Eq. (28), the mass transfer coefficient that cancels the intrinsic reactance is obtained from,

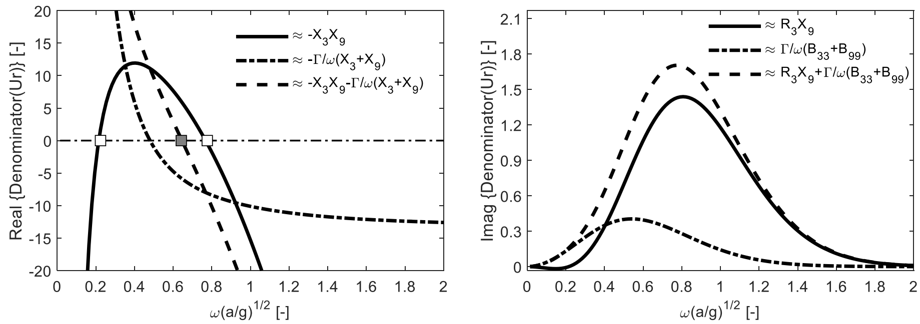

Fig. 3. Breakdown of the real part (left) and imaginary part (right) of the denominator of the relative velocity complex amplitude for a**xisymmetric two-body self-reacting heaving WECs**, considering the simplifications discussed above. On the left: additional resonance, represented by the gray square mark (located between the two white squa2res corresponding to the natural frequencies of each of the two bodies), caused by mass transfer. On the right: increased damping due to mass transfer.

$$\Gamma = -\omega\frac{X_3X_9}{X_3+X_9}, \tag{29}$$

and thus, the complex amplitude of the mass that needs to be transferred between the two bodies to theoretically cancel the intrinsic reactance is given by,

$$g\widehat{m}_t \cong \Gamma\widehat{z}_r = -\omega\frac{X_3X_9}{X_3+X_9}\widehat{z}_r. \tag{30}$$

Fig. 3 shows the effect of integrating a MTM to modify de reactance of two-body WECs. As expected, the figure shows, on the left, an additional resonance, caused by the mass transfer, among the resonance frequency of body 1 (at lowest frequency) and body 2 (at the highest frequency). This new resonance frequency, marked by the gray square mark in the left graphics, is verified for a constant mass transfer coefficient, Γ. Therefore, theoretically, a frequency-dependent Γ, could further cancel the reactance over a wider range, significantly increasing the capture width.

3.2. Power take-off equipment

Up to this point, we have studied the dynamics of free-floating systems without equipment for converting wave energy into electricity. Although, to fully describe the WEC behavior we need to include a mechanism with which the absorbed energy by the primary converter is transformed into useable electricity, i.e., a power take-off (PTO) equipment. By doing so, and applying the discussed assumptions and simplifications to the two-body WEC design explored here, Eq. (27) becomes

$$U_r = \frac{F_0}{Z_i+Z_{pto}} = \frac{i(F_3X_9-F_9X_3)}{\left[-X_3X_9-\Omega(X_3+X_9)+R_{pto}R_3\right]+i\left[R_3X_9+R_9X_3+\Omega R_3+R_{pto}(X_3+X_9)\right]}, \tag{31}$$

where the PTO impedance, $Z_{pto} = R_{pto} + iK_{pto}$, consists of a resistance, R_{pto}, which enables electricity generation, and a capacitive reactance, K_{pto}. Moreover, $\Omega = \Gamma/\omega + K_{pto}$ represents the combined capacitive reactance associated with the MTM and the PTO. Unlike the previous assumptions in Eqs. (22) and (27), the term R_9X_3, in the imaginary part of the denominator in Eq. (31) was not omitted, despite typically being much smaller than R_3X_9, as explained in Section 2.1.2 (see Eq. (19)). This is justified because the term R_9X_3 becomes dominant (despite being very small, since $R_9 \cong 0$) whenever X_9 is zero or very close to zero, situation in which the resonance of the reaction spar's heave motion in self-reacting two body WECs occurs. Thus, by considering the term R_9X_3 in Eq. (31) we avoid a singularity at the frequency that cancels the reaction spar's reactance ($X_9 = 0$) under optimal absorption conditions, as we will see below.

From Eq. (31), the average useful power capture can be written as

$$\overline{P}_a = \frac{1}{2}R_{pto}|U_r|^2 = \frac{1}{8}\frac{|F_0|^2}{R_i}\frac{4\mu}{(1+\mu)^2(1+\lambda^2)}, \tag{32}$$

where, in accordance with Eq. (13), F_0 is given by,

$$F_0 = \frac{i(F_3X_9-F_9X_3)}{R_3+i(X_3+X_9)}, \tag{33}$$

and the dimensionless parameters λ and μ are defined by

$$\lambda = \frac{X_i}{R_i+R_{pto}} \tag{34}$$

and

$$\mu = \frac{R_{pto}}{R_i}, \tag{35}$$

the first representing the ratio between the intrinsic reactance of the WEC and its resistance (i.e., the relationship between the energy stored and the energy dissipated per cycle), while the second reflects the relative importance of the PTO load resistance compared to the WEC's inherent energy dissipation (hydrodynamic damping). The resistive and the reactive components of the inherent impedance, R_i and X_i, are obtained, according to Eq. (15), from

$$R_i = \frac{R_3X_9^2+R_9X_3(X_3+X_9)}{R_3^2+(X_3+X_9)^2} \cong R_3\left(\frac{X_9}{X_3+X_9}\right)^2 + R_9\frac{X_3}{X_3+X_9}, \tag{36}$$

and

$$X_i = \frac{X_3X_9(X_3+X_9)+\Gamma/\omega\left[R_3^2+(X_3+X_9)^2\right]}{R_3^2+(X_3+X_9)^2} \cong \frac{X_3X_9}{X_3+X_9}+\frac{\Gamma}{\omega}. \tag{37}$$

As with a single-body systems, optimal power absorption is achieved when the PTO impedance has a reactance that cancels the intrinsic reactance and a resistance that matches the equivalent single-body hydrodynamic damping, in other words, the PTO impedance is equal to the complex conjugate of the intrinsic impedance, i.e.,

$$Z_{pto} = Z_i^* = \frac{Z_3^* Z_9^* - Z_c^{*2}}{Z_0^*}. \tag{38}$$

In this context, $Z_{pto} = R_{pto} + i(K_{pto} + \Gamma/\omega)$, assuming it includes both resistive and reactive components, with the MMT contributing to the latter. According to Eq. (32), the optimal PTO damping and spring coefficients (including the mass transfer effect) that theoretically maximize power harvesting, are given, respectively, by

$$R_{pto_{opt}} = \frac{R_3X_9^2 + R_9X_3^2 + R_9X_3X_9}{R_3^2 + (X_3 + X_9)^2} \cong R_3\left(\frac{X_9}{X_3 + X_9}\right)^2, \tag{39}$$

and

$$\Omega_{opt} = \frac{\Gamma}{\omega} + K_{pto_{opt}} = -\frac{R_3^2X_9 + X_3X_9(X_3 + X_9) + R_3R_9X_3}{R_3^2 + (X_3 + X_9)^2} \cong -\frac{X_3X_9}{(X_3 + X_9)}. \tag{40}$$

Eqs. (39) and (40) establish that maximum energy capture is achieved when the combined hydrodynamic damping equals the PTO resistive load, i.e., $R_{pto} = R_i$, provided the WEC is resonant, i.e., $X_i = 0$ (which also implies $\lambda = 0$). As an additional validation of Eqs. (39) and (40), it is insightful to analyze the hypothetical case, without mass transfer, in which the reaction spar in self-reacting two-body systems has a very large inertia (which restrains its motion), effectively reducing the WEC working principle to a single body (floater) oscillating vertically. In this case, Eqs. (39) and (40) show that both coefficients of the PTO load impedance, R_{pto} and K_{pto}, would converge to values that cancel the intrinsic impedance of a single body, so that the converted power is maximized (i.e., $R_{pto} = R_3$ and $K_{pto} = -X_3$, when $m_9 \rightarrow \infty$), which is a well-established theoretical result in the field of wave energy.

Fig. 4 shows the frequency dependence of the resistive and reactive coefficients under optimal capture conditions for the two-body WECs considered. It can be observed that the combined capacitive reactance, Ω_{opt}, (from both the PTO spring, K_{pto}, and the MTM, Γ/ω) required to cancel the system's intrinsic reactance for optimal power capture is:

i) **positive** for frequencies below the natural frequency of the reaction spar -body 2- (left white dot) and thus, theoretically, the reactance can be canceled by the 'negative spring' effect from mass transfer, which counteracts the hydrostatic stiffness, S. However, energy capture is of little relevance in this frequency range, and thus the benefit of mass transfer is limited, since the intrinsic hydrodynamic radiation is very low, and accordingly, the optimal PTO resistance is also minimal, as Fig. 4 illustrates.
ii) **negative** within the frequency range between the natural frequencies of the reaction spar -body 2- (left white dot) and the combined body (gray dot). Therefore, it is needless to transfer mass among both bodies since it acts as a 'negative spring' and, within this range, the reactance must be canceled with a 'positive spring' provided by the PTO or any other auxiliary system.
iii) **positive** between the natural frequencies of the combined body (gray dot) and the floater -body 1- (right white dot) which means that the reactance can be canceled with a 'negative spring' effect resulting from mass transfer. It is important to note that this frequency range is typically the most relevant for energy absorption since the floater -body 1- is the body with greater resistive capabilities (higher hydrodynamic damping), which is essential for effective wave energy capture.
iv) **negative** for frequencies above the floater -body 1- natural frequency (left white dot) and thus, theoretically, the reactance must be canceled with a 'positive spring' effect provided by the PTO or any other additional auxiliary system. Nevertheless, in this frequency range, wave energy capture is less significant due to the low energy content of the waves.

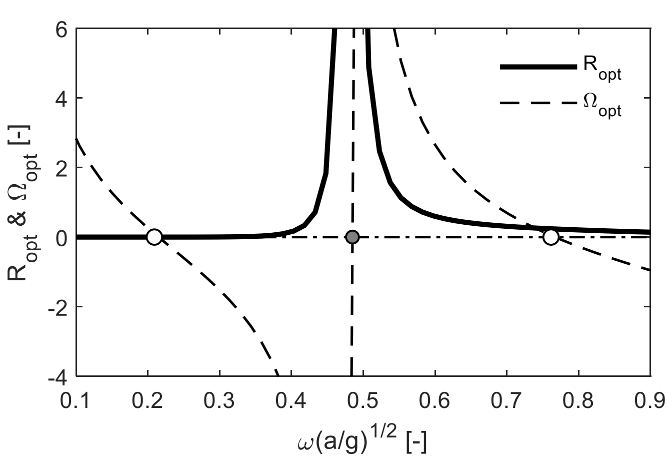

Fig. 4. PTO resistive/damping coefficient (R_{opt}) and reactive/spring coefficient (Ω_{opt}) for two-body self-reacting systems under optimal wave energy capture conditions.

Eqs. (39) and (40) reflect the simplification that reactance dominates over resistance (i.e., $R_3 < X_3 + X_9$ and thus $R_3^2 \ll (X_3 + X_9)^2$. While this assumption breaks down near the combined body resonance frequency, it remains valid in practice since energy capture is negligible at that point, as the WEC behaves as a single rigid body, with no relative motion between the spar and floater, causing the optimal PTO damping to approach infinity, as shown in Fig. 4.

From this point forward, we assume that the PTO introduces only resistive loads, and therefore, the reactive coefficient K_{pto} is neglected to isolate the potential impact of MTM on the WEC's performance. Under these circumstances, the mass transfer is the only effect that counteracts the capacitance's ability of the hydrostatic spring-like system to store potential energy, leading to a less stiff device. Theoretically, a PTO system could be designed to cancel the WEC's intrinsic reactance, as previously discussed, functioning as a spring when inductive reactance outweighs capacitive reactance, or as a 'negative spring' otherwise. In this way, the PTO could enable the WEC to operate in resonance under any condition. However, to better interpret the potential impact of mass transfer and its 'negative spring' effect, that possibility is not considered here.

In optimal wave energy capture conditions, the equivalent excitation force F_0 is in phase with the relative velocity, U_r, given by

$$U_{r_{opt}} \cong \frac{F_3X_9 - F_9X_3}{2(R_3X_9^2 + R_9X_3^2)}(X_3 + X_9) \tag{41}$$

As anticipated, Eq. (41) shows that the optimal relative velocity, $U_{r_{opt}}$, becomes zero at the frequency corresponding to the combined body resonance, where $X_3 + X_9 = 0$. As hydrodynamic pressure decreases with depth, the excitation loads on the reaction spar are significantly reduced, and thus $F_9 \ll F_3$. This could lead to disregarding the second term in the numerator of Eq. (41); however, this simplification was not considered because, in certain circumstances, $X_9 \ll X_3$, which reduces the impact of the significantly higher excitation loads acting on the WEC floater. Similarly, following the same reasoning, we might consider omitting the second term in the denominator, $R_9X_3^2$, but despite its relevance around the frequency that cancels the reaction spar's reactance ($X_9 = 0$), suppressing it originates a singularity at that frequency, which is unrealistic. By applying the reciprocity relation for axisymmetric bodies in deep waters (where the depth function $D(kh) \cong 1$), which states that $R_{3,9} = \omega k |f_{3,9}|^2 / 2\rho g^2$ (with $f_{3,9} = F_{3,9}/A$ being the heave excitation force coefficient) and after straightforward mathematical manipulation, the optimal converted power can be expresses as

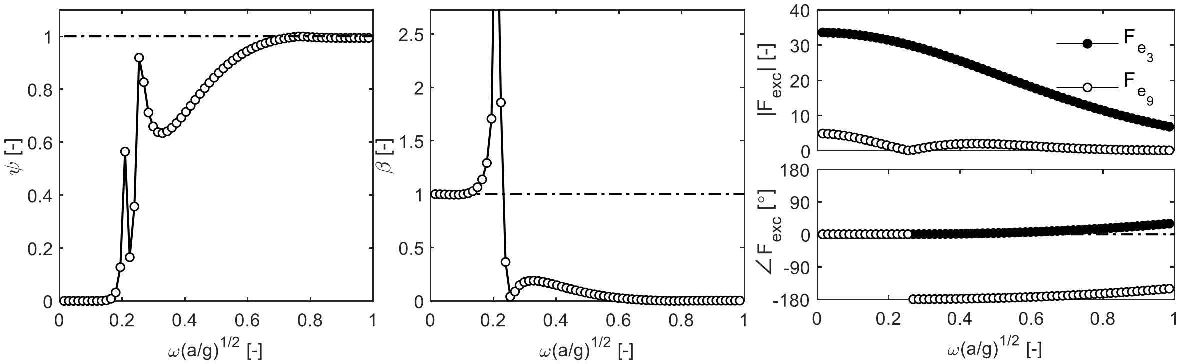

Fig. 5. Power reduction factor, ψ, for a generic self-reacting two-body spar-type WEC (left) and the corresponding β coefficient (middle), both influenced by the excitation forces on the two bodies, shown in terms of the magnitude and phase of their complex amplitude (right).

$$P_{opt} = \frac{1}{8}\frac{|F_0|^2}{R_i} \cong \frac{|F_3|^2}{8R_3}\psi, \tag{42}$$

where ψ is a coefficient, ranging between 0 and 1, representing the power reduction factor for two-body systems, defined by

$$\psi = \frac{(1-\beta)^2}{1+\beta^2}, \tag{43}$$

in which

$$\beta = \frac{F_9}{X_9}\frac{X_3}{F_3} \tag{44}$$

It is important to note that in the mathematical derivation of Eq. (42) it was assumed that $\beta = |\beta|$. The validity of this assumption is supported by the fact that the complex amplitude of the excitation forces on both bodies, F_3 and F_9 (per unit incident wave amplitude), are approximately real (besides the fact that F_3 and F_9 exhibit a phase lag of roughly 0° or 180°), as shown in Fig. 5 (right), which leads to the conclusion that β is real. In addition, F_9 and X_9 generally have opposite signs, as both reverse sign at resonance. As the reactance typically dominates over resistance, we can state that below the resonance frequency $F_9 > 0$ and $X_9 < 0$, with X_9 primarily governed by hydrostatic stiffness. The opposite occurs at frequencies above resonance, where X_9 is primarily dominated by inertial effects. Applying the same reasoning to F_3 and X_3 we can conclusion that β is real and positive and tend to zero tends to zero for high frequencies. Therefore, we can ultimately conclude that $\beta \geq 0$, as shown in Fig. 5 (middle), which implies that $(1-\beta)^2/(1-\beta^2) \leq 1$, as illustrated in Fig. 5 (left). This highlights the well-known result that the optimal converted power of a two-body system does not exceed that of a single-body system. In Fig. 5, white and black dots in the right subplot represent the simulated frequencies, where a very small step of 0.015 rad/s was considered.

Eq. (43) shows that the coefficient β must be zero for a two-body system to reach the theoretical maximum power absorption of a single-body WEC, a limit that cannot be exceeded, regardless of the number of bodies in the system, as represented in Fig. 5. Notably, the design approach adopted here makes achieving β values close to zero relatively straightforward, as the excitation force on the reaction spar is of small amplitude ($F_9 \ll F_3$) due to its depth. To some extent, the β-dependent ratio in Eq. (43) acts as a correction due to the presence of a second body.

The optimal absorption condition may result in unrealistic WEC oscillations, as optimal velocity amplitude scales with the equivalent excitation force, F_0, which in turn depends on the amplitude of the incident waves. Therefore, optimal absorption is only feasible when wave amplitudes remain below the WEC's designed maximum stroke limit. For larger values of F_0, or higher incident waves, the velocity amplitude must be upper bounded, i.e., $U_{max} < U_{opt}$, [18,31]. Whenever this restricted condition is applicable, the suboptimal maximum time average converted power is obtained from,

$$\overline{P}_{s-opt} = \frac{1}{2}\frac{|F_0|}{R_i}U_{max} - \frac{1}{2}R_i U_{max}^2. \tag{45}$$

After lengthy but straightforward algebraic manipulation, Eq. (45) takes the form,

$$\overline{P}_{s-opt} \cong \frac{1}{8}\frac{|F_3|^2}{R_3}\frac{(1-\beta)^2}{1+\beta^2}\left(1-|\nu-1|^2\right), \tag{46}$$

where ν denotes the ratio between the upper bounded and the optimal velocity, i.e., $\nu = U_{max}/U_{opt}$.

The parentheses on the right-hand side of Eq. (46) quantify the reduction in potential converted power imposed by the amplitude constraint, relative to the unconstrained case in Eq. (42). Consistent with Eq. (46), the absorption width, defined as the ratio of converted power to the incident wave-energy transport per unit frontage, J, is given by,

$$L_{c_{s-opt}} = \frac{P_{r_{opt}}}{J} \cong \frac{1}{k}\frac{(1-\beta)^2}{1+\beta^2}\left(1-|\nu-1|^2\right). \tag{47}$$

The optimal absorption width for spar-type two-body systems occurs for $\nu = 1$, matching the theoretical maximum of a single body whenever $\beta = 0$. Similarly, the dimensionless power absorption is defined as the ratio of the suboptimal converted power to the theoretical maximum of a single-body system, i.e.,

$$P^*_{s-opt} \cong \frac{(1-\beta)^2}{1+\beta^2}\left(1-|\nu-1|^2\right). \tag{48}$$

Assuming that the upper limit of the relative velocity is imposed solely by the PTO load resistance, which means that mechanical end-

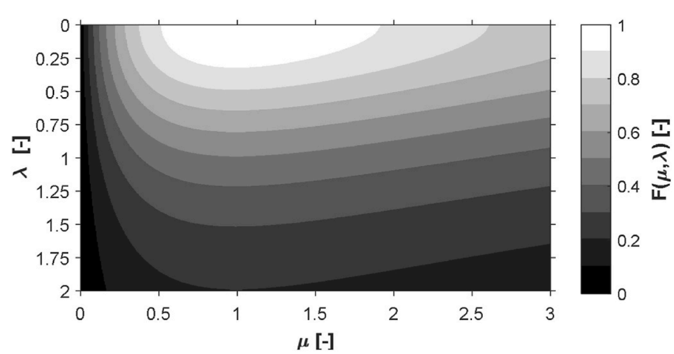

Fig. 6. Grayscale colormap showing the controller-dependent component as a function of both the ratio between PTO load resistance and the WEC's inherent energy dissipation (hydrodynamic damping), μ, and the ratio between the intrinsic reactance and the overall WEC resistance, λ.

stops are not required, the dimensionless power capture in Eq. (48) can be rewritten, using Eq. (32), as

$$P^*_{s-opt} \cong \frac{(1-\beta)^2}{1+\beta^2}\frac{4\mu}{(1+\mu)^2(1+\lambda^2)}, \tag{49}$$

where the dimensionless parameters μ and λ are defined by Eqs. (34) and (35), respectively. When the PTO load impedance is either purely real or, if complex, unable to cancel the intrinsic reactance, the converted power is maximized when $R_{pto} = |Z_i|$, which generalizes the specific case presented in Eq. (42). In these non-optimal conditions, the μ- and λ-dependent fraction in Eq. (49) reduces to $2/(1+\mu)$.

For the most general case, Eq. (49) and Eq. (42), shows that the WEC performance is governed by three contributions: a shape-independent component, $|F_3|^2/(8R_3)$, representing the theoretical maximum for a single-body system; a shape-dependent factor, $(1-\beta)^2/(1+\beta^2)$, reflecting a conceptual limitation inherent to the energy extraction from the relative motion between two bodies; and a controller-dependent component, $4\mu/\left[(1+\mu)^2(1+\lambda^2)\right]$, illustrated in Fig. 6, which captures the additional constraint arising from the inability to fully cancel reactance and match the PTO resistance to the intrinsic hydrodynamic damping across the entire frequency spectrum.

Regardless of the case, maximizing power capture requires minimizing λ, which is naturally canceled at three frequencies when the transfer mass mechanism is disabled, namely, when the reactance of body 1 or body 2 is canceled (i.e., $X_3 = 0$ or $X_9 = 0$), and at the combined body resonance (i.e., $X_3 = -X_9$), as shown in Fig. 4. If the MTM is well-designed, it will shift the resonant frequencies, minimizing λ near the resonances of body 1 and body 2, while leaving the combined body resonance unaffected, where λ remains zero with or without mass transfer. This can be readily verified by substituting into Eq. (34) the intrinsic resistance and reactance of the two-body WEC, defined in terms of each body's resistive and reactive components, as given by Eq. (36) and Eq. (37), respectively. By doing so, and after some mathematical manipulation, the dimensionless parameter λ can be rewritten as

$$\lambda = \frac{(X_3+\Gamma/\omega) + 2\Gamma\big/\omega(X_3/X_9) + (X_9+\Gamma/\omega)(X_3/X_9)^2}{(R_3+R_{pto}) + 2R_{pto}(X_3/X_9) + (R_9+R_{pto})(X_3/X_9)^2} \cong \frac{X_3+\Gamma/\omega}{R_3+R_{pto}}. \tag{50}$$

In Eq. (50) it was assumed, for practical reasons, that the potential widening of the capture bandwidth caused by the mass transfer is predominantly centered around the resonance of body 1, as it is the primary contributor to the radiation characteristics of the WEC, and thus $X_3/X_9 \cong 0$. Absorption near the resonance of body 2 is generally of minor practical relevance (despite potentially being high in theory) because its hydrodynamic radiation is limited. This is mainly due to its geometry and, more importantly, the depth of its center of gravity. Consequently, achieving effective energy absorption in this region would require unrealistically high motion amplitudes. Accordingly, the singularity in Eq. (50) (when $X_9 = 0$) is disregarded, since the frequency range of interest does not include the resonance frequency of body 2.

3.2.1. *Capture bandwidth widening*

In the frequency range neighboring the resonance frequency of the floater (body 1), the relative absorbed power response, $P^*(\omega)/P^*(\omega_0)$, is obtained from,

$$\frac{P(\omega)|F_3(\omega_0)|^2}{P(\omega_0)|F_3(\omega)|^2} \cong \frac{1}{1+\lambda^2}, \tag{51}$$

where, for simplicity, the frequency dependence of the radiation resistance, R_i, was neglected (near the resonance frequency), and $\beta \cong 0$ was assumed, given that X_3 is close to zero. Defining the capture bandwidth, $\Delta\omega = \omega_r - \omega_l$, as the frequency interval where the relative absorbed power response, Eq. (51), exceeds 1/2 (denoting the right and left side of this frequency interval by the subscripts *r* and *l*, respectively) and thus $-1 \leq \lambda \leq 1$, the relative capture bandwidth related to the floater dynamics is then given by,

$$\frac{\Delta\omega}{\omega_{0_r}} = \frac{\omega_r-\omega_l}{\omega_{0_r}} \cong \frac{\delta_r+\delta_l}{\omega_{0_r}} + \left[1-(1-\alpha)^{1/2}\right], \tag{52}$$

where the subscript 0 in ω_{0_r} and ω_{0_l} (with $\omega_{0_l} = \omega_{0_r}(1-\alpha)^{1/2}$), denotes the rightmost and leftmost resonance frequencies, respectively. Similarly, $\delta_{r,l}$ are the corresponding damping coefficients, given by $\delta = (R_{pto}+R_3)/[2(m_3+A_{33})]$ (see Ref. [16]), and $\alpha = \Gamma/C_3$ represents the mass transfer ratio ($0 \leq \alpha < 1$). Eq. (52) shows that without mass transfer (i.e., $\alpha = 0$ and thus $\omega_{0_l} = \omega_{0_r}$) the relative capture bandwidth becomes $2\delta_r/\omega_{0_r}$ (see Ref. [16]).

To simplify the evaluation of the gain in energy capture due to mass transfer, Eq. (52) is reformulated as an inequality,

$$\frac{\Delta\omega}{\omega_{0_l}} \geq \frac{1}{(1-\alpha)^{1/2}}\left[\frac{2\delta_r}{\omega_{0_r}} - (1-\alpha)^{1/2} + 1\right]. \tag{53}$$

In eq. (59), it is assumed that the right damping coefficient, δ_r, is typically smaller than the left one, δ_l, since $R_{pto}+R_3$ is usually higher near the left resonance frequency, while m_3+A_{33} remains nearly constant due to the small variations in the added mass coefficient. The first term inside the square brackets of Ineq. 59 is the only one that remains when the MTM is disconnected. If the MTM operates passively, with no control over mass transfer (i.e., α is constant), there is always a gain, as $\Delta\omega/\omega_{0_l} > 2\delta_r/\omega_{0_r}$. In this scenario, the device's natural frequency can be more effectively tuned to the incoming waves without increasing its inertia or relying on auxiliary mechanisms with a similar purpose. Although, additional gains in energy production can be achieved if the mass transfer can be properly controlled, which requires adjusting α as a function of frequency ($0 \leq \alpha(\omega) < 1$). In such case, Fig. 7 maps the percentage of potential bandwidth expansion, as expressed by Eq. (53), for upper limits of the mass transfer factor, α, on the x-axis, relative to the characteristic absorption bandwidth of conventional point absorbers (without the mass transfer feature), given by the relative capture bandwidth, $2\delta_r/\omega_{0_r}$, on the y-axis.

The white square in Fig. 7 highlights the bandwidth expansion enabled by mass transfer within the most likely range of mass transfer factors, α, and typical capture bandwidths (normally quite narrow) of conventional point absorbers (with no mass transfer). Fig. 7 shows that, when the mass transfer mechanism is well controlled, the proposed mass transfer mechanism can increase the power capture bandwidth by more than three times. As expected, it is visible that the bandwidth widening increases for higher mass transfer factors and smaller relative bandwidths. Therefore, when the WEC's capture bandwidth is broadened using other control strategies/reactance control mechanisms, the impact of mass transfer becomes negligible. On the contrary, for very narrow capture bandwidths, the effect of mass transfer is substantial. To highlight this effect, Fig. 8 shows the bandwidth widening, considering a mass transfer factor, $\alpha \leq 0.2$, in self-reacting WECs. It is important to note that the discussion here aims to illustrate the potential benefits of mass transfer in improving WEC performance, but no design optimization has been conducted.

Fig. 8 shows the contour lines corresponding to different percentages by which the dimensionless absorber power exceeds the theoretical maximum (right side plot - with proper mass transfer control; left side plot without mass transfer mechanism). This figure presents graphically the expansion of the bandwidth, showing that even small mass transfer factors - $\alpha \leq 0.2$ - can significantly expand the capture bandwidth, as μ varies up to the point of zero power absorption, if a well-controlled mass transfer mechanism is implemented. In the study case presented, the expansion of the bandwidth where the absorber power exceeds 90 % of the theoretical maximum corresponds to an increase of approximately 190 % when comparing the device with MTM to the non-MTM

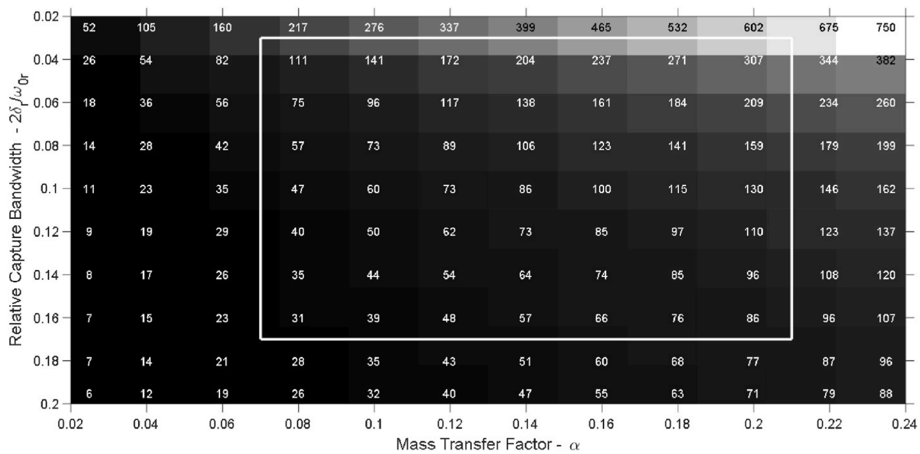

Fig. 7. Grayscale colormap showing the power capture bandwidth increase (in percentage) enabled by a well-controlled mass transfer mechanism.

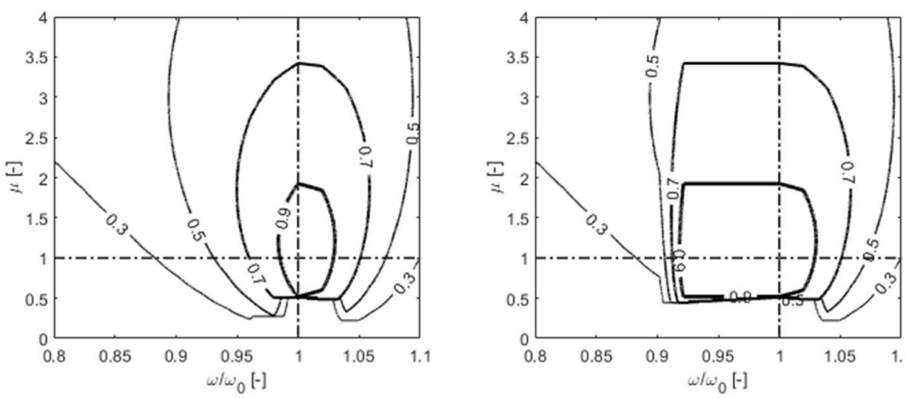

Fig. 8. Frequency response equipotential lines that outline the areas where the dimensionless absorber power exceeds 30 %, 50 %, 70 %, and 90 % of the theoretical maximum as a function of the normalized PTO loads, μ, in a self-reacting WEC with vertical excursions below the floater radius. The left side shows the power absorption without mass transfer, while the right illustrates the bandwidth widening under proper mass transfer control (with $\alpha \leq 0.2$).

configuration. The ability to control the mass flux between both bodies is not trivial and will be addressed in the continuation of this work, nevertheless if no control is considered (i.e., α is constant) the resonant frequency will decrease, self-tuning the concept without resort to reactive energy from an external source (or additional inertia).

Active control strategies, such as optimal control in two-body point absorbers [22,23,25], have demonstrated significant performance improvements (e.g., a ~20 % increase in absorbed energy compared to constant damping control using MPC [23], or a 9 % increase in annual yield with an inverse model controller [23]). Nevertheless, these benefits can result in negative net energy when losses inherent to bidirectional reactive control (e.g., generator losses [30]) are overlooked, and their effectiveness remains highly dependent on the accuracy of prediction algorithms.

To address this limitation, several proposals incorporate additional mechanical elements to tune resonance and enhance energy capture and/or bandwidth, such as pneumatic spring systems [28] or pendulum-based inertial elements [29]. These approaches passively extend the resonance interval, enabling broadband absorption through multiple resonance bands (multi-peak responses). The proposed MTM aligns with this class of approaches, seeking to broaden the capture bandwidth and tune it to typical ocean wave periods. Although these studies are essentially theoretical, relying on multiple simplifications and assumptions, the findings suggest that MTM enables a substantial quantitative increase in bandwidth (up to 190 % expansion, where the absorber power exceeds 90 % of the theoretical maximum, as Fig. 8 illustrates), achieving effects comparable to those reported in Ref. [29], while requiring less structural complexity.

It is worth noting that this study is limited to a conceptual analysis of the MTM's potential to improve energy extraction in point absorbers, specifically by broadening the bandwidth. As the analysis is conducted in the frequency domain, future work should address more detailed dynamic modeling, time-domain simulations, and techno-economic assessments. Additionally, the development and control of practical mechanisms for mass transfer between bodies in real WECs remains an open challenge. Finally, while the mass transfer coefficient (α) can theoretically range from 0 to 1, practical designs should limit transferred mass to avoid unfeasible configurations that compromise the model's assumptions.

4. Conclusions

This study investigates a theoretical concept aimed at broadening the inherently narrow absorption bandwidth of point absorbers, thereby enhancing their performance. In such WECs, the capacitive reactance (i.e., the ability of the hydrostatic spring to store potential energy) dominates over the inductive reactance (i.e., the mass's ability to store kinetic energy) in typical sea states, making it hard to cancel the mechanical reactance using conventional means. To overcome this, the proposed approach investigates a 'negative spring' effect (i.e., a force acting with the motion) enabled by mass transfer between the two bodies of a spar-type, axisymmetric, two-body heaving WEC.

The study concludes that controlled mass transfer between the two bodies of spar-type point absorbers can significantly widen the capture bandwidth (more than three times the power capture bandwidth in the study case presented, and nearly double the bandwidth even with small mass transfer factor, i.e. the amount of mass transferred by the mechanism is small with respect to the total stiffness), even with minimal mass, potentially tripling it. In the absence of control (i.e., with a constant mass transfer factor), the mechanism can still provide a valuable self-tuning effect, reducing the resonant frequency without increasing the inertia or relying on external reactive power, thus offering promising economic advantages.

Mass transfer positively influences the frequency range between the natural frequencies of the combined body and the floater, where a negative spring effect is needed to cancel the system's intrinsic reactance. This frequency range is typically the most critical for energy absorption, as the floater must be designed with optimal hydrodynamic resistive capabilities, which is essential for effective wave energy capture. Within the frequency range between the natural frequency of the reaction spar and that of the combined body, mass transfer between the two bodies of the WEC is unnecessary. Instead, reactance must be canceled by a positive spring effect provided by the PTO or an auxiliary system.

A single-body WEC, where an axisymmetric floater oscillates vertically around a fixed concentric structure exchanging mass with it, represents a special case of the two-body self-reacting system analyzed in this study. For this case, the derived expressions still apply by assuming $m_9 \gg m_3$, $F_9 \cong 0$ and, accordingly, $R_9 \cong 0$, leading to optimal power conversion when $R_{pto} = R_3$ and $K_{pto} = -X_3$, which is a well-established result in wave energy research. In these conditions, for frequencies below the floater's natural frequency, the required compensating reactance to cancel the intrinsic reactance is negative and can, in theory, be supplied by the 'negative spring' effect of mass transfer. It is worth noting that the floater can be designed to resonate near the upper end of the wave spectrum and tuned to prevailing sea states through controlled mass transfer. In this case, the frequency range above the floater's natural frequency (where intrinsic reactance must be canceled by a positive spring from the PTO) is considered less relevant due to the lower energy content of those waves.

A WEC design approach that effectively implements a 'negative spring' effect, without the need for complex auxiliary systems, is under study and will be detailed in an upcoming publication. Alongside conventional two-body point absorbers that transfer mass via connected internal tanks filled with water or other fluids, floating two-body OWCs, where the second body is the water column itself, have also been considered. Moreover, further investigation is required to validate the effectiveness of the proposed approach, which defines the next steps of this research. These may include analysis such as: impact of mass transfer on the dynamic stability of two-body spar-type heaving point absorbers; CFD analysis to examine water flow patterns around the WEC and the effects of potential vortex shedding; Techno-economic assessment to evaluate the cost-effectiveness and potential benefits of the mass transfer feature; time-domain numerical modeling of the WEC dynamic response to understand the impact of mass transfer between the two bodies and explore strategies for controlling the non-linear mass flux, with special attention is given to the convolution that arises between frequency-dependent mass flux and relative displacement.

Although the methodology developed in this study focuses on nearshore-to-offshore spar-type two-body heaving point absorbers, it can be readily adapted to other types of wave energy converters with different operating principles, provided the goal is to broaden the absorption bandwidth.where β represents the wave incidence angle and J the wave-energy transport per unit frontage (for a pure progressive wave, $J = \rho g^2 D(kh)|A|^2/(4\omega)$ with A denoting the wave amplitude and $D(kh)$ the depth function, which approaches 1 in deep waters). For an axisymmetric two-body WEC constrained to vertical oscillations, as considered here, the excitation force is independent of β, leading to the simplification of the general radiation-resistance matrix into the form given in Eq. (17).

CRediT authorship contribution statement

Marco Alves: Writing – review & editing, Writing – original draft, Visualization, Validation, Supervision, Software, Investigation, Funding acquisition, Formal analysis, Conceptualization. **António Sarmento:** Writing – review & editing, Supervision, Funding acquisition, Formal analysis, Conceptualization. **Marcos Blanco:** Writing – review & editing, Writing – original draft, Validation, Methodology, Conceptualization. **Miguel Vicente:** Methodology, Investigation, Formal analysis, Data curation, Conceptualization. **Mário Vieira:** Writing – original draft, Software, Methodology, Investigation, Formal analysis, Data curation, Conceptualization. **Marcos Lafoz:** Writing – review & editing, Supervision, Project administration, Funding acquisition, Conceptualization.

Declaration of competing interest

The authors declare that they have no known competing financial interests or personal relationships that could have appeared to influence the work reported in this paper.

Acknowledgements

This work was conducted as part of the activities of the research groups participating in the REMAR thematic network (Opportunities for the Integration of Ocean Energies into Ibero-American Electric Grids – https://www.cyted.org/remar), promoted and supported by the Ibero-American Programme of Science and Technology for Development (CYTED). The work also benefited from funding provided by the Recovery and Resilience Plan of Portugal (PRR) and the European Union's NextGenerationEU funds to WavEC, through the multi-year funding scheme for the 2022–2025 triennium, in recognition of its status as a Portuguese CTI – Technology and Innovation Center – by the National Innovation Agency (ANI), an entity under the Ministry of Economy.

References

[1] M. Perez, R. Perez, Update 2022 – a fundamental look at supply side energy reserves for the planet, Solar Energy Advances 2 (2022) 100014, https://doi.org/10.1016/j.seja.2022.100014.
[2] D. Magagna, et al., Wave and tidal energy strategic technology agenda [Online]. Available: https://www.policyandinnovationedinburgh.org/wave-and-tidal-energy-strategic-technology-agenda.html, 2014.
[3] JCR, Facts and Figures on Offshore Renewable Energy Sources in Europe, 2020.
[4] J. Elvinger, et al., Special Report: Offshore Renewable Energy in the EU - Ambitious Plans for Growth but Sustainability Remains a Challenge, 2023, https://doi.org/10.2865/85796.
[5] A. LiVecchi, et al., Exploring Opportunities for Marine Renewable Energy in Maritime Markets, U.S. Department of Energy (DOE), 2019.
[6] IRENA, Innovation Outlook: Ocean Energy Technologies, 2020. Abu Dhabi (UAE).
[7] J. Hodges, et al., An international evaluation and guidance: framework for ocean energy technology. https://www.ocean-energy-systems.org/publications/oes-documents/market-policy-/document/an-international-evaluation-and-guidance-framework-for-ocean-energy-technology/, 2023.
[8] S.H. Salter, J.R.M. Taylor, N.J. Caldwell, Power conversion mechanisms for wave energy, Proc. IME M J. Eng. Marit. Environ. 216 (1) (Jan. 2002) 1–27, https://doi.org/10.1243/147509002320382103.
[9] A.A. Faiad, I.A. Gowaid, Linear generator technologies for wave energy conversion applications: a review, in: 2018 53rd International Universities Power Engineering Conference (UPEC), IEEE, Sep. 2018, pp. 1–6, https://doi.org/10.1109/UPEC.2018.8542007.
[10] E. Tedeschi, M. Molinas, Wave-To-Wave Buoys Control for Improved Power Extraction Under electro-mechanical Constraints, 2010, https://doi.org/10.1109/ICSET.2010.5770274.
[11] A. Blavette, D.L. O'Sullivan, T.W. Lewis, M.G. Egan, Dimensioning the equipment of a wave farm: energy storage and cables, Industry Applications, IEEE Transactions on 51 (3) (2015) 2470–2478, https://doi.org/10.1109/TIA.2014.2382754.
[12] A. Blavette, D.L. O'Sullivan, R. Alcorn, T.W. Lewis, M.G. Egan, Impact of a medium-size wave farm on grids of different strength levels, Power Systems, IEEE Transactions on 29 (2) (Mar. 2014) 917–923, https://doi.org/10.1109/TPWRS.2013.2284513.

[13] M. Göteman, J. Engström, M. Eriksson, J. Isberg, Optimizing wave energy parks with over 1000 interacting point-absorbers using an approximate analytical method, International Journal of Marine Energy 10 (Jun. 2015) 113–126, https://doi.org/10.1016/j.ijome.2015.02.001.

[14] M. Blanco, et al., Recent advances in direct-drive power take-off (DDPTO) systems for wave energy converters based on switched reluctance machines (SRM), in: A. Samad, S. Sannasiraj, V. Sundar, P. Halder (Eds.), Ocean Wave Energy Systems. Ocean Engineering & Oceanography, vol. 14, Springer, Cham, 2022, pp. 487–532, https://doi.org/10.1007/978-3-030-78716-5_17, ch. 17.

[15] M. Rosati, J.C.C. Henriques, J.V. Ringwood, Oscillating-water-column wave energy converters: a critical review of numerical modelling and control, Energy Convers. Manag. X 16 (Dec. 2022) 100322, https://doi.org/10.1016/j.ecmx.2022.100322.

[16] I. Villalba, M. Blanco, J.I. Pérez-Díaz, D. Fernández, F. Díaz, M. Lafoz, Wave farms grid code compliance in isolated small power systems, IET Renew. Power Gener. 13 (1) (Jan. 2019) 171–179, https://doi.org/10.1049/iet-rpg.2018.5351.

[17] J. Falnes, Ocean Waves and Oscillating Systems, Linear Interactions Including Wave-Energy Extraction, Cambridge University Press, Cambridge, 2002.

[18] J. Falnes, Wave-energy conversion through relative motion between two single-mode oscillating bodies, J. Offshore Mech. Arctic Eng. 121 (1) (Feb. 1999) 32–38, https://doi.org/10.1115/1.2829552.

[19] L. Hai, M. Goteman, M. Leijon, A methodology of modelling a wave power system via an equivalent RLC circuit, IEEE Trans. Sustain. Energy 3029 (c) (Oct. 2016), https://doi.org/10.1109/TSTE.2016.2538803, 1–1.

[20] L. Thévenin, Sur un nouveau théorème d'électricité dynamique (On a new theorem of dynamic electricity), C. R. Hebd. Seances Acad. Sci. 97 (1883) 159–161.

[21] J. Hals, J. Falnes, T. Moan, A comparison of selected strategies for adaptive control of wave energy converters, J. Offshore Mech. Arctic Eng. 133 (2011) 31101, https://doi.org/10.1115/1.4002735.

[22] M. Yetkin, S. Kalidoss, F.E. Curtis, L.V. Snyder, A. Banerjee, Practical optimal control of a wave-energy converter in regular wave environments, Renew. Energy 171 (Jun. 2021) 1382–1394, https://doi.org/10.1016/j.renene.2021.02.134.

[23] C. Hall, W. Sheng, Y. Wu, G. Aggidis, The impact of model predictive control structures and constraints on a wave energy converter with hydraulic power take off system, Renew. Energy 224 (Apr. 2024) 120172, https://doi.org/10.1016/j.renene.2024.120172.

[24] H. Wang, V. Wijaya, T. Zeng, Y. Zhang, Deep reinforcement learning-based non-causal control for wave energy conversion, Ocean. Eng. 311 (Nov. 2024) 118860, https://doi.org/10.1016/j.oceaneng.2024.118860.

[25] J.M. Silva, S.M. Vieira, D. Valério, J.C.C. Henriques, GA-optimized inverse fuzzy model control of OWC wave power plants, Renew. Energy 204 (Mar. 2023) 556–568, https://doi.org/10.1016/j.renene.2023.01.039.

[26] Y. Lu, H. Zhang, J. Zhou, X. Li, P. Li, D. Xu, A bistable point absorber wave energy convertor with a mechanical motion rectifier, Ocean. Eng. 289 (Dec. 2023) 116246, https://doi.org/10.1016/j.oceaneng.2023.116246.

[27] H. Liu, L. Huang, Y. Li, J. Yang, J. Zhang, Resonance control to eliminate reactive power of an improved dual-port direct-drive wave energy converter, Ocean. Eng. 288 (Nov. 2023) 116007, https://doi.org/10.1016/j.oceaneng.2023.116007.

[28] A. Cotten, A. Kurniawan, V.S. Neary, R.G. Coe, G. Bacelli, A compressible degree of freedom as a means for improving the performance of heaving wave energy converters, Renew. Energy 227 (Jun. 2024) 120421, https://doi.org/10.1016/j.renene.2024.120421.

[29] G. Giorgi, Embedding parametric resonance in a 2:1 wave energy converter to get a broader bandwidth, Renew. Energy 222 (Feb. 2024) 119928, https://doi.org/10.1016/j.renene.2023.119928.

[30] M. Blanco, P. Moreno-Torres, M. Lafoz, D. Ramírez, Design parameters analysis of point absorber WEC via an evolutionary-algorithm-based dimensioning tool, Energies 8 (10) (Oct. 2015) 11203–11233, https://doi.org/10.3390/en81011203.

[31] G. Bacelli, J. V Ringwood, A geometric tool for the analysis of position and force constraints in wave energy converters, Ocean. Eng. 65 (2013) 10–18, https://doi.org/10.1016/j.oceaneng.2013.03.011.

[32] IRENA, Offshore renewables: an action agenda for deployment, Abu Dhabi (UAE), https://www.irena.org/publications/2021/Jul/Offshore-Renewables-An-Action-Agenda-for-Deployment, 2021.

[33] E. Al Shami, R. Zhang, X. Wang, E. Al Shami, R. Zhang, X. Wang, Point absorber wave energy harvesters: a review of recent developments, Energies 12 (1) (Dec. 2018) 47, https://doi.org/10.3390/en12010047.

[34] C.-H. Lee, J.N. Newman, X. Zhu, AN extended boundary integral equation method for the removal of irregular frequency effects, Int. J. Numer. Methods Fluid. 23 (7) (Oct. 1996) 637–660, https://doi.org/10.1002/(SICI)1097-0363(19961015)23:7<637::AID-FLD437>3.0.CO, 2-3.

[35] A. Babarit, G. Delhommeau, Theoretical and numerical aspects of the open source BEM solver NEMOH, in: Proceedings of the 11th European Wave and Tidal Energy Conference, Nantes, France, 2015. Proceedings of the 11th European Wave and Tidal Energy Conference, https://hal.science/hal-01198800.